Fully Automatic, Retrospective Enhancement of Real-Time Acquired Cardiac Cine MR Images Using Image-Based Navigators and Respiratory Motion-Corrected Averaging

Peter Kellman,[1]* Christophe Chefd'hotel,[2] Christine H. Lorenz,[3] Christine Mancini,[1] Andrew E. Arai,[1] and Elliot R. McVeigh[4]

Real-time imaging may be clinically important in patients with congestive heart failure, arrhythmias, or in pediatric cases. However, real-time imaging typically has compromised spatial and temporal resolution compared with gated, segmented studies. To combine the best features of both types of imaging, a new method is proposed that uses parallel imaging to improve temporal resolution of real-time acquired images at the expense of signal-to-noise ratio (SNR), but then produces an SNR-enhanced cine by means of respiratory motion-corrected averaging of images acquired in real-time over multiple heartbeats while free-breathing. The retrospective processing based on image-based navigators and nonrigid image registration is fully automated. The proposed method was compared with conventional cine images in 21 subjects. The resultant image quality for the proposed method (3.9 ± 0.44) was comparable to the conventional cine (4.2 ± 0.99) on a 5-point scale (*P* = not significant [n.s.]). The conventional method exhibited degraded image quality in cases of arrhythmias whereas the proposed method had uniformly good quality. Motion-corrected averaging of real-time acquired cardiac images provides a means of attaining high-quality cine images with many of the benefits of real-time imaging, such as free-breathing acquisition and tolerance to arrhythmias. Magn Reson Med 59:771–778, 2008.

Key words: MRI; heart; real-time; parallel MRI; SENSE; navigator; motion correction; nonrigid; myocardial function; regional wall motion

Real-time imaging may be used to image cardiac function and flow without breathholding or ECG triggering (1–4), and might be important in patients with congestive heart failure or in pediatric cases. Real-time imaging is also beneficial in cases of arrhythmia. which is problematic for conventional gated, segmented cine imaging. However, real-time imaging typically has compromised spatial and temporal resolution compared with gated, segmented breathheld studies. Real-time imaging with improved spatial and/or temporal resolution maybe achieved using parallel imaging (5–8) at the expense of trading signal-to-noise ratio (SNR) for increased acquisition speed, thereby reducing image quality.

To combine the best features of both types of imaging, a new method is proposed that produces an SNR-enhanced cine from images acquired in real-time by means of respiratory motion-corrected averaging. Fully automated, retrospective processing of real-time acquired images is based on image-based navigators and nonrigid image registration. A similar approach has been validated for ECG-triggered, free-breathing delayed enhancement imaging at a single cardiac phase (9,10).

Free-breathing cardiac imaging with respiratory gating may be implemented using navigator echoes (11,12), which track the position of the diaphragm. Data are accepted or rejected based on an acceptance window, which is typically several millimeters. Prospective slice-following techniques (13) improve the image quality by adjusting for heart motion within the acceptance window, thereby allowing a somewhat increased window with higher acquisition efficiency. However, the motion of the heart does not strictly track the diaphragm during free-breathing (14), which limits the dependence on simple models and linear motion-correction factors. Furthermore, use of conventional navigator echoes is problematic for continuous cine imaging due to the overhead time required to generate the navigator signal and due to interruption of the steady state. Self-navigator approaches have been demonstrated for cardiac cine imaging using radial acquisition (15,16), as well as three-dimensional (3D) Cartesian approaches (17,18), which rely on profiles derived by repeated sampling through the center of *k*-space. Nevertheless, dependence on a simple motion model still limits the image quality. Self-navigated techniques have not yet been reported for real-time imaging.

The proposed approach is based on real-time image acquisition and strictly retrospective processing. In order to combine images from multiple heart beats during free-breathing, a navigator signal derived from the images is used to define an acceptance window. In-plane respiratory-induced distortion of the heart within the acceptance window is corrected using a nonrigid deformation. Prospective slice-following is not incorporated, therefore

[1]Laboratory of Cardiac Energetics, National Heart, Lung and Blood Institute, National Institutes of Health, Department of Health and Human Services, Bethesda, Maryland, USA.

[2]Siemens Corporate Research, Princeton, New Jersey, USA.

[3]Siemens Corporate Research, Baltimore, Maryland, USA.

[4]Johns Hopkins University School of Medicine, Department of Biomedical Engineering, Baltimore, Maryland, USA.

Grant sponsor: Intramural Research Program of the NIH, National Heart, Lung and Blood Institute, and a Cooperative Research and Development Agreement between the National Heart, Lung and Blood Institute and Siemens Medical Solutions.

*Correspondence to: Peter Kellman, Laboratory of Cardiac Energetics, National Institutes of Health, National Heart, Lung and Blood Institute, 10 Center Drive, MSC-1061, Building 10, Room B1D416, Bethesda, MD. E-mail: kellman@nih.gov

Received 2 August 2007; revised 10 October 2007; accepted 20 November 2007.

DOI 10.1002/mrm.21509
Published online in Wiley InterScience (www.interscience.wiley.com).

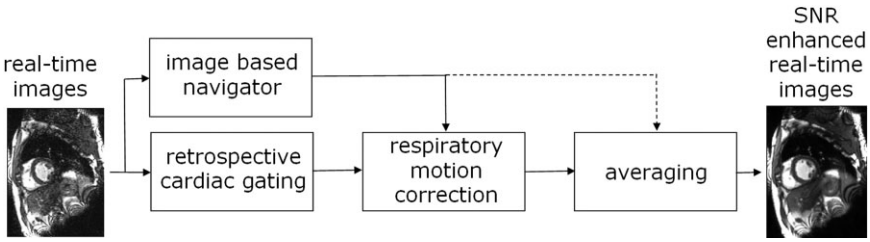

FIG. 1. Retrospective processing of real-time acquired images to enhance SNR by respiratory motion-corrected averaging.

through-plane affects are determined by the acceptance window.

The proposed approach has several benefits including simplifying the acquisition by eliminating the time and complexity of setting up a navigator scan. Ghosting artifacts that result from residual respiratory motion during the segmented acquisition are also eliminated. Furthermore, real-time imaging is insensitive to variations in RR interval (time duration between two consecutive R waves of the ECG) and arrhythmia rejection may be incorporated into retrospective averaging.

METHODS

Proposed Strategy

The basic strategy for the proposed approach is to acquire a series of images for a number of cardiac cycles during free-breathing, correct the respiratory motion using a nonrigid warping, and average images to produce a cardiac cine with improved SNR. The processing steps for this approach (Fig. 1) are as follows: 1) perform retrospective processing to cardiac-gate the images based on simultaneously acquired ECG data; 2) perform respiratory motion correction at each cardiac phase; and 3) average motion-corrected images at each cardiac phase to create a cardiac cine series with enhanced SNR. An image-based navigator is used to drive the selection of which heart beat is used as a reference for image registration in the respiratory motion-correction step, and may also be used for selective averaging to determine which images are within the desired respiratory window. Details of each step in this process are described in greater detail in the following sections.

Real-Time Imaging

Real-time imaging was performed on 1.5T Siemens Avanto and Espree scanners (Siemens Medical Solutions, Erlangen, Germany), using a steady-state free precession (SSFP) (true fast imaging with steady precession [true-FISP]) sequence. Parallel imaging was used to provide rate 4 acceleration using sensitivity encoding (SENSE) incorporating temporal filtering (TSENSE) for auto-calibration (7). For the Avanto with 200 T/m/s max slew rate, the temporal resolution was 35 ms for a 128 $\times$ 60 matrix, BW = 1395 Hz/pixel (TR = 2.3 ms), and it was 56 ms for a 192 $\times$ 80 matrix with BW = 1000 Hz/pixel (TR = 2.8 ms). For the Espree with 100 T/m/s max slew rate, the temporal resolution was 44 ms for a 128 $\times$ 60 matrix, BW = 1150 Hz/pixel (TR = 2.9 ms), and it was 65 ms for a 192 $\times$ 80 matrix with BW = 814 Hz/pixel (TR = 3.25 ms, asymmetric echo). The image FOV was typically 360 $\times$ 270 cm^2 (75% rectangular FOV), which corresponded to a typical in-plane spatial resolution of 1.9 $\times$ 3.4 mm^2 for the 192 $\times$ 80 matrix. Slice thickness was 6 mm.

Images were reconstructed online, and were postprocessed offline using MATLAB®. Raw data and ECG log files were saved for analysis of ECG triggering, and for calibrated SNR measurement (19). Raw data contained a time stamp (2.5 ms precision) of each echo (*k*-space line) as well as the time from the preceding ECG trigger, which was used for retrospective cardiac gating of the images. Acquisitions were 16 s in duration, allowing for up to approximately 16 averages depending on the heart rate.

Image Registration

Nonrigid registration was performed pairwise between a target and reference image (Fig. 2). Nonrigid registration

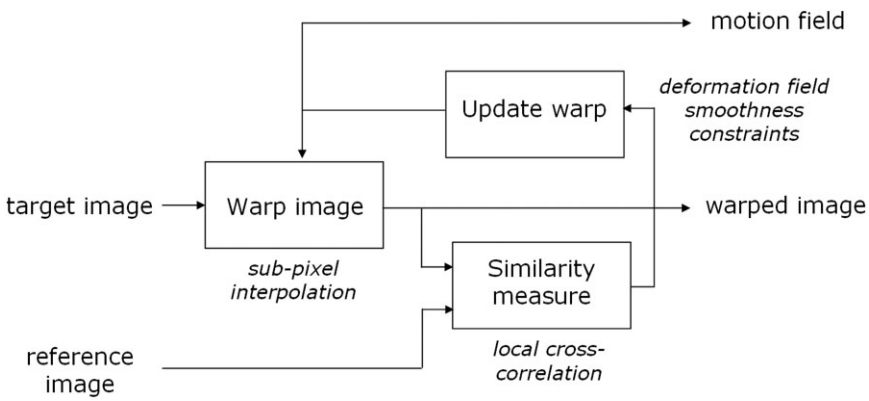

FIG. 2. Nonrigid image registration between target and reference images using intensity-based similarity measure and subpixel interpolation for image warping.

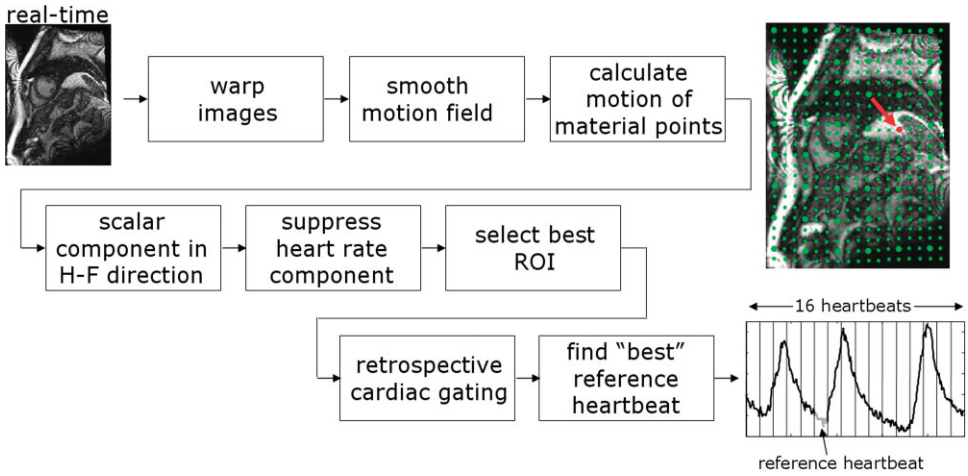

FIG. 3. Calculation of image-based navigator signal used for determining "best" reference heart beat for motion correction and for selective averaging. The navigator signal is derived from the motion field used to warp the real-time acquired images to the initial reference frame. The tissue region selected for navigator signal is indicated by an arrow (red).

was used since it both outperformed rigid body registration in the heart region, and could be fully automated without user interaction to specify bounding regions (10). For each pair, the algorithm (20,21) estimates a deformation that maximizes the local cross-correlation between the reference and the uncorrected (target) image. The local cross-correlation criterion was selected for its robustness to intensity changes, signal inhomogeneities, and noise. The resulting algorithm is intensity-based and does not require the extraction and selection of anatomical landmarks. The deformation is modeled as a smooth vector field that gives for each pixel on the reference its corresponding location on the target image. The algorithm recovers the deformation by composition of small displacements, incrementally maximizing the similarity criterion. This process, which can be seen as the numerical implementation of a transport equation, provides a large capture range. The smoothness of the deformation is imposed by applying a low-pass filter to the vector field increments. The process is implemented in a multiscale approach from coarse to fine resolution (in four steps of two), which increases the speed and provides improved convergence. Once the nonrigid motion (deformation) field is estimated, the images are warped using a subpixel spline-based interpolator. The method used was selected since the implementation was highly optimized for speed. Alternative nonrigid registration methods such as a spline model for deformation (10) might be used.

The image registration is performed twice. Registration is used initially to calculate the image-based navigator described next and in the determination of the which heartbeat will be used as a reference for the final image registration. The final image registration used for respiratory motion correction is performed on the images after cardiac gating involving temporal interpolation and uses the reference heartbeat that has the least respiratory motion, determined from the initial processing. In the final image registration, the target and reference images are from the same cardiac phase but at different heartbeats and this process is repeated for each cardiac phase.

Image-Based Navigators

A navigator signal proportional to the respiratory motion was used to determine the "best" reference heartbeat for a final image registration used for motion correction. The navigator was also used to determine which images were within the acceptance window for selective averaging. A nonrigid registration (warping) was performed on the complete time series of images for the purpose of extracting the motion field. A subsequent second-pass image registration will be performed for final motion correction. The first-pass image registration is used for calculating the image-based navigator signal and arbitrarily used the first image as the reference for registration. The processing steps (Fig. 3) were as follows: 1) warp images using the previously described nonrigid registration to generate a vector motion field (at each pixel); 2) smooth the motion field by spatial low-pass filter to reduce noise; 3) calculate the motion of material points in the forward direction (i.e., from reference frame to target); 4) compute the scalar motion component in the head-foot direction based on the image orientation; 5) mask regions that have a strong heart rate component in the scalar motion signal; 6) select the best region as having the largest signal variance; 7) cardiac-gate the navigator signal using the recorded ECG R-wave trigger time to calculate a fixed number of interpolated samples corresponding to the calculated image times; and 8) determine the "best" heartbeat from the navigator signal as having the minimum root-mean-squared distance (averaged over each heartbeat) from the most frequent position as determined from peak in histogram of the navigator signal. The complete process is performed automatically. An example image (Fig. 3, inset) illustrates the warping of the material points (arbitrary 17 $\times$ 23 green grid points overlayed in image) for a fixed time frame. The material 6 $\times$ 8 larger size grid points represent the approximate centers of the smooth regions used (i.e., the images were subdivided into 6 $\times$ 8 regions for subsequent analysis). The navigator signal was selected from these 6 $\times$ 8 regions (Fig. 4) as the signal with largest power excluding the regions with strong heart rate component. Each of the signals was fast Fourier transformed (FFTd) and the presence of a heart rate component in the 45–150-bpm range was analyzed (signals from masked regions are shaded in Fig. 4). The presence of the heart rate component was due to the fact that the nonrigid registration was attempting to warp cardiac motion, registering each frame to a fixed phase. The output navigator signal was resampled to the

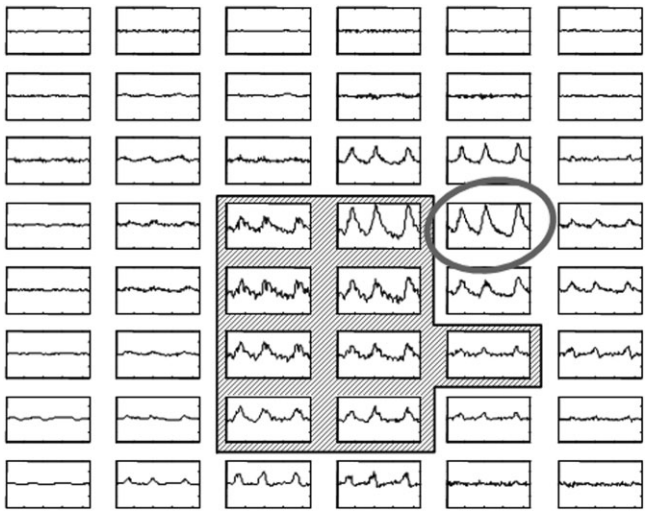

FIG. 4. Navigator signals calculated in each subregion of the image. Circled signal waveform represents the navigator from automatically selected region. Shaded plots represent the signals with significant heart components that are excluded. The horizontal time axis spans 16 s and the vertical axis is tissue displacement, spanning 12 mm.

cardiac trigger and a single heartbeat was selected to use as a reference for the final image registration (Fig 3). The navigator signal is measured in units of distance. The navigator is the measured displacement (in the superior/inferior [S/I] direction) as measured by the motion field, which is the tissue displacement in the automatically selected region-of-interest (ROI). The ROI does not necessarily correspond to the diaphragm as in conventional navigators, although in the example of Fig. 3 the tissue region selected for the navigator signal indicated by the red arrow is close to the diaphragm position.

Retrospective Cardiac Gating

Images and the image-derived navigator signal were retrospectively cardiac-gated using ECG-trigger times embedded in the raw data. Cardiac gating and temporal interpolation are performed prior to the final image registration step used for respiratory motion correction so that the same cardiac phase from each heartbeat may be registered. The time for each image (center of *k*-space) was recorded to 2.5 ms precision. The input image times of real-time acquired images are asynchronous with the cardiac timing and it was desired to calculate output images (and navigator samples) for a fixed number of cardiac phases. A piecewise linear interpolation approach (22) was used, which maintained a constant output sample rate during systole and stretched or shrunk the diastolic portion to match the average RR interval (Fig. 5). The systolic and diastolic periods were based on the average RR interval (22). Output images at the prescribed sample times were calculated using linear interpolation in the image domain on a pixelwise basis. The input frame rate using a 192 $\times$ 80 matrix size was either 18 or 15 frames/s, corresponding to the Avanto and Espree MR imagers, respectively. The results in this work used 30 calculated output phases.

Respiratory Motion-Correction

Respiratory motion-correction was applied to the retrospectively cardiac-gated images using the nonrigid registration described above. For each cardiac phase, multiple images at various respiratory positions were registered with a reference image of the same cardiac phase chosen from the heartbeat that had the most frequent respiratory position, based on histogram analysis of the navigator signal (described above). Image registration only compensated respiratory motion since it was gated to the cardiac phase. The respiratory position vs. cardiac phase of the reference heartbeat was generally fairly constant by virtue of the method used to choose the reference. Any residual motion tended to be slowly varying. A prior method that attempted to choose a more optimum reference for each phase selected from different heartbeats tended to result in nonsmooth, discontinuous motion, and thus this approach was not used.

Selective Averaging

Averaging of the motion-corrected images (Fig. 6) was used to improve the image SNR. Selective averaging was

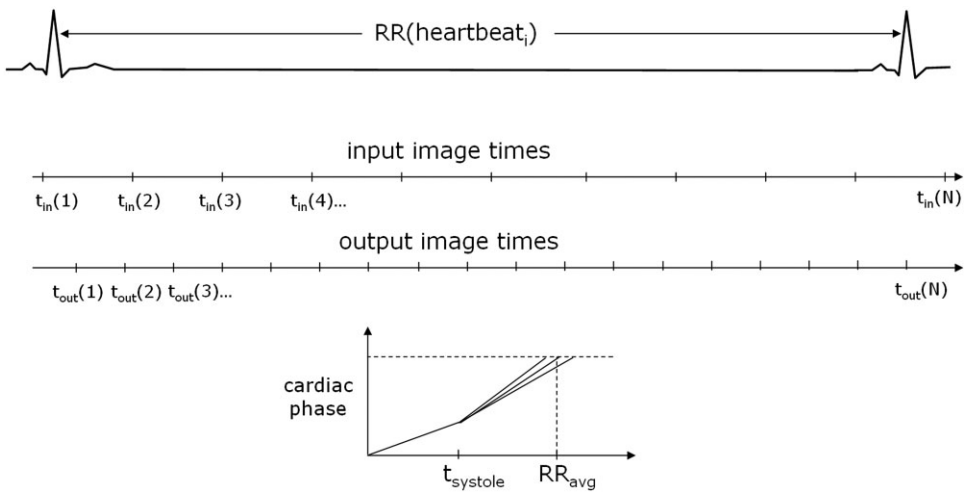

FIG. 5. Retrospective cardiac triggering using piecewise linear interpolation to stretch each heartbeat to fit the average RR interval using model based on average heart rate (22).

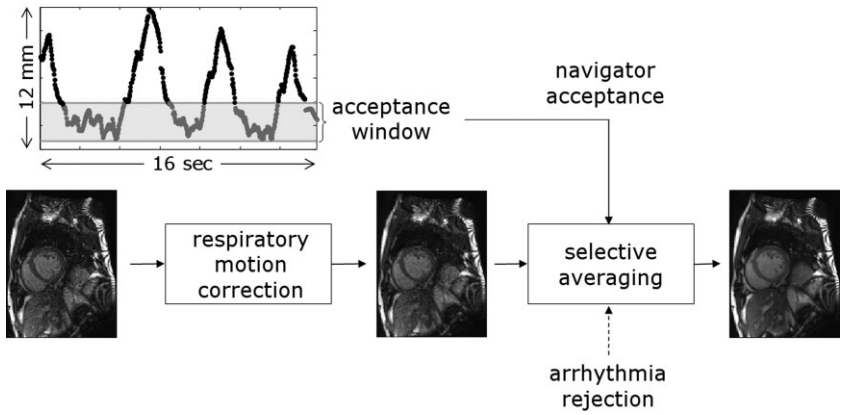

FIG. 6. Motion-corrected averaging to enhance SNR of real-time acquired images.

performed based on the image-based navigator signal, or optionally on all images as a special case. For navigator-based selective averaging, the acceptance criterion was a fixed percentage of the peak-to-peak variation, although a fixed displacement might also be used. A 25% acceptance window was used. In the example of Fig. 6 with normal breathing, the acceptance window was 2.7 mm with approximately 45% navigator efficiency (percent accepted). The window was centered about the most frequent respiratory position as determined by histogram analysis of the navigator signal.

Additionally, arrhythmia rejection could also be used to exclude irregular heartbeats or missed triggers, as determined retrospectively. In patients that had an arrhythmia, a simple arrhythmia rejection scheme was used in which dissimilar heartbeats or heartbeats with short RR interval or premature ventricular contractions were manually discarded from the selective average.

Experimental Measurements

Imaging was performed in patients ($N = 18$) with suspected coronary artery disease or known chronic myocardial infarction (MI) and healthy volunteers ($N = 3$) under clinical research protocols approved by the Institutional Review Boards of the National Heart, Lung, and Blood Institute and Suburban Hospital, with written informed consent. To characterize the performance of image registration and subpixel interpolation, the standard deviation (SD) of edge positions (four endo- and four epicardial edges) in intensity profiles (Fig. 7) through the left ventricular (LV) myocardium was measured for motion-corrected images across all heartbeats (typically 16 beats depending on heart rate) at both end-diastolic and end-systolic phases. SNR was compared in images with and without averaging in four myocardial ROIs. Measurement of the SNR improvement and variation in edge profiles was made on the first $N = 6$ subjects. Navigator efficiency was measured as the percentage of total acquired images accepted for averaging.

Enhanced real-time acquired images during free-breathing were compared with conventional, breathheld, gated, segmented cine imaging. Parameters for conventional cine imaging were as follows: 1.5T Siemens Espree scanner, SSFP sequence, ECG-triggered, retrospectively gated, matrix size = 256 × 156, views-per-segment = 13, TR = 3.37 ms, bandwidth = 930 Hz/pixel. The temporal resolution was 43.8 msec with 30 phases calculated retrospectively. Using parallel imaging at rate 2 with generalized autocalibrating partially parallel acquisitions (GRAPPA) with 44 center lines for autocalibration, there were 104 lines (slight phase encoded [PE] oversampling) acquired in eight heartbeats, resulting in nine heartbeat breathhold duration with one discarded acquisition.

Image quality for all subjects was assessed by two experts using a 5-point scale (with increment = $\frac{1}{2}$) as described below. Conventional breathheld, ECG-gated segmented images and enhanced real-time acquired images for the corresponding slice were scored separately, presented in a blinded, randomized manner. The rating was based on: 1) SNR and image artifacts; 2) readability of global function; 3) readability of regional function; and 4) ability to discern fine details such as chordal structures, valve leaflets, and LV trabeculation. A score of 5 (excellent) was assigned when all four aspects were rated as excellent, i.e., without artifacts, high contrast between blood and myocardium, and sharp borders and strong appearance of fine structural details. A score of 4 (good) was assigned when all aspects were rated as good, with some fine structures visible, but not necessarily all, and possibly mild artifacts. A score of 3 (fair) meant that the image quality was sufficient to read regional wall motion

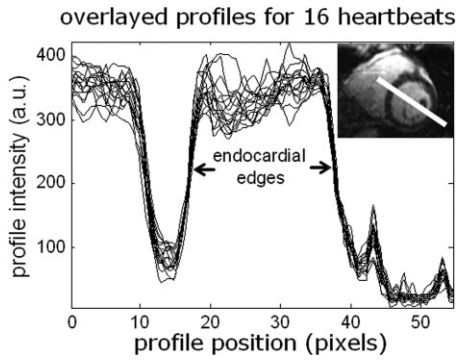

FIG. 7. Example signal intensity profiles across the LV of motion-corrected images (see profile for inset image) for 16 heartbeats at end-diastole. Measurement of SD of 4 myocardial edges for two orthogonal profiles at both systolic and diastolic phases for six subjects was SD = 0.26 ± 0.16 pixels.

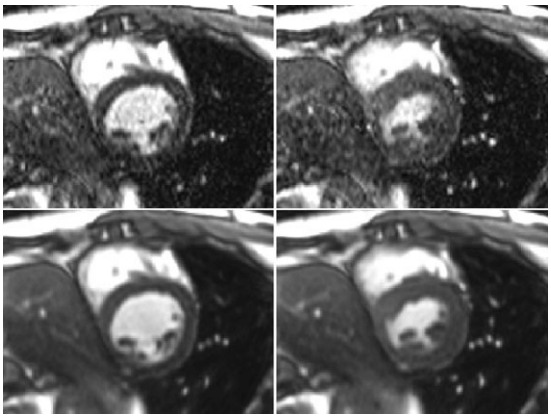

FIG. 8. Real-time acquired images for patient with chronic MI with respiratory motion-corrected averaging (bottom) and without averaging (top) for end-diastolic (left) and end-systolic (right) phases.

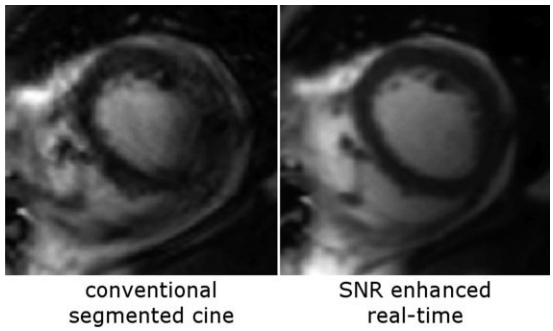

FIG. 10. Example cardiac cine images for patient with arrhythmia (atrial fibrillation) comparing conventional gated segmented cine (left) with SNR enhanced cine (right). Arrhythmia-induced artifacts evident in the segmented cine are not present in the real-time acquired cine. Arrhythmia rejection was used in both cases.

but that one or more aspect was suboptimal. A score of 2 (poor) meant that one or more aspect was seriously impaired, leading to inability to read regional function. Images rated with a score of 1 were considered nondiagnostic when regional and global function could not be determined.

RESULTS

The image registration performance was measured on $N = 6$ subjects including normal volunteers ($N = 2$) and patients ($N = 4$) with chronic MI. The SD of edge positions was 0.26 ± 0.16 pixels (for all 8 edges × 2 phases × 6 subjects). These images used a matrix size of 192 × 80 with typical in-plane resolution of 1.9 × 3.4 mm^2; therefore, a 0.26-pixel variation corresponded to 0.5 mm in readout direction and 0.9 mm in phase encode direction. The typical motion prior to correction was approximately 4 mm. The average myocardial SNR improved with averaging within several percent of the expected $\sqrt{N_{avg}}$ gain. The navigator efficiency was 43 ± 8% (mean ± SD, $N = 18$).

Cine images are shown for two patients with chronic MI (Fig. 8 and 9). Images (Fig. 8) show clearer definition of the epicardial border (posterior wall) and papillary muscles after averaging. SNR-enhanced images (Fig. 9) (right) have comparable image quality to conventional breathheld cine images (left), and approximately 3:1 improvement in SNR over raw real time images (center) (case corresponds to Fig. 6 navigator with 45% averaging efficiency). The regional wall motion abnormalities apparent on the original images were also apparent on the motion-corrected averaged images.

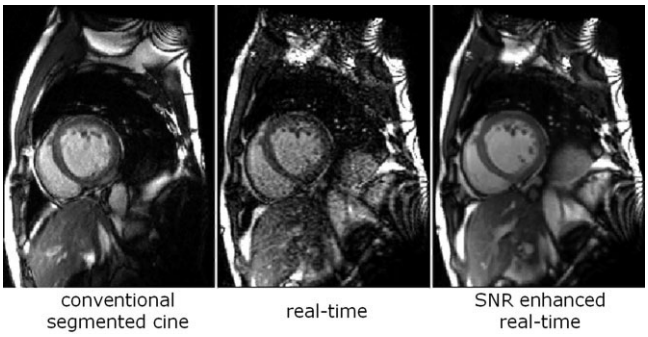

FIG. 9. Example images comparing conventional gated segmented cine (left), raw real-time acquired images (center), and SNR-enhanced cine (right) for second patient with chronic MI.

In the case of a patient with atrial fibrillation (Fig. 10), real-time images were acquired for a duration of 30 s. Following retrospective gating and motion correction, 10 heartbeats were manually selected to average based on their similarity. The conventional segmented cine used the vendor provided product sequence with arrhythmia rejection enabled. The enhanced cine images are free of the arrhythmia-induced artifacts evident in the conventional breathheld, segmented cine.

The image quality score was 4.2 ± 0.99 (mean ± SD, $N = 21$ subjects) for conventional, segmented breathheld cine, and 3.9 ± 0.44 (mean ± SD) for enhanced real-time acquired images, with no statistically significant difference between expert readers. All enhanced real-time acquired images had image quality scores in the range 3–4.5, whereas the conventional cine images had a much wider variation (Fig. 11) ranging from 1.5 to 5. Conventional cine images scored poorly in cases of arrhythmia ($N = 3$) whereas the same cases scored much better for enhanced real-time acquired cine images. Conventional cine images had higher temporal and spatial resolution (35 ms and 256 × 144 matrix) than the enhanced cine images, which resulted in several cases with excellent rating for conventional cine images due to visibility of fine structures, whereas the corresponding lower resolution enhanced real-time acquired cine were rated as only very good due to the lack of visibility of fine structures. Nevertheless, the more uniform quality of the enhanced images were comparable on the average to the standard cine images and sufficient to assess cardiac function in all cases.

DISCUSSION

The proposed technique combines nonrigid motion correction with image based navigators for selective averag-

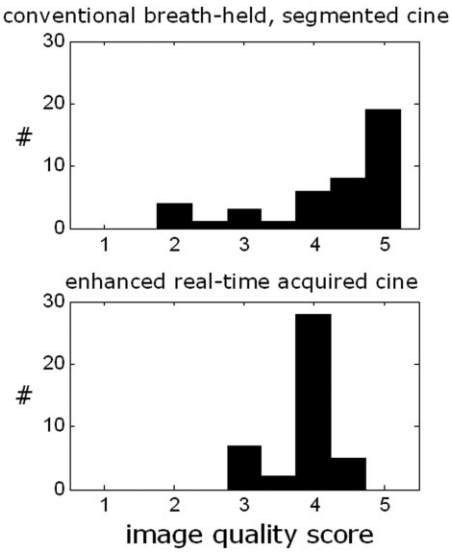

FIG. 11. Histograms of image quality scores (21 subjects × 2 readers) for conventional, breathheld segmented cine image (top) and enhanced real-time acquired cine images (bottom), illustrating larger variation in image quality for conventional cine images with no statistical significance in average quality.

ing. Image-based navigators are calculated retrospectively, and therefore, do not permit prospective slice tracking to limit through-plane motion. Nevertheless, through-plane motion may be limited to an acceptable level based on the acceptance window. Unlike conventional navigators, the proposed approach compensates for in-plane motion and nonrigid distortion. Using conventional navigators, residual in-plane motion may lead to both loss of resolution and respiratory artifacts. In the future, there is the potential to derive image-based navigators in real-time with low latency and perform prospective slice tracking, if desired.

In the proposed approach, images are acquired in a free running manner without ECG triggering and are retrospectively gated based on recorded ECG-triggered times. It might be possible to use cardiac self-gating (23) and eliminate the dependence on ECG signal. While only simple arrhythmia rejection was employed for the cases studied here, retrospective processing permits the possibility of more sophisticated ECG recognition algorithms.

Spatial and temporal resolution of the real-time images with parallel imaging (acceleration rate, $R = 4$) was still compromised as compared to breathheld segmented cine. However, with optimized coil arrays it might be possible to increase the acceleration rate further (e.g., $R = 6$), incurring a greater loss in SNR yet still achieving reasonable image quality after averaging. As the SNR of the raw real-time images drops to unity or below, then the averaging efficiency is effectively degraded since averaging must also make up for magnitude detection loss. As real-time volumetric coverage becomes possible, this method may be further extended using volume registration.

The current study compared the proposed enhanced real-time acquired method with the existing conventional cine protocol used clinically by our institution. This protocol uses a larger matrix size for better depiction of fine structures. A protocol with reduced matrix size and correspondingly decreased breathhold duration would indeed reduce sensitivity to poor breathholding but would still not be capable of free-breathing, and thus was not considered in this study. Our goal was to assess how well the proposed free-breathing technique would perform as compared to our current standard. A conventional segmented cine protocol with reduced matrix size might decrease the variation in quality due to breathholding difficulty observed in conventional cine, as shown in the histogram in Fig. 11 (top). Furthermore, arrhythmia rejection discards heartbeats and extends the acquisition, thereby exacerbating breathholding problems. Additionally, the experience with arrhythmia rejection at our institution is that in many cases it is not effective.

CONCLUSIONS

Motion-corrected averaging of real-time acquired cardiac images provides a means of attaining high-quality cine images with many of the benefits of real-time imaging, such as free-breathing acquisition and tolerance for arrhythmias. A byproduct of the proposed method is the image based navigator, which has potential to additionally be used for cardiorespiratory-resolved imaging. Significant SNR enhancement was achieved without apparent loss of resolution on all subjects studied. The free-breathing acquisition may be extended in duration to gain further SNR.

REFERENCES

1. Setser RM, Fischer SE, Lorenz CH. Quantification of left ventricular function with magnetic resonance images acquired in real time. J Magn Reson Imaging 2000;12:430–438.
2. Plein S, Smith WH, Ridgway JP, Kassner A, Beacock DJ, Bloomer TN, Sivananthan MU. Qualitative and quantitative analysis of regional left ventricular wall dynamics using real-time magnetic resonance imaging: comparison with conventional breath-hold gradient echo acquisition in volunteers and patients. J Magn Reson Imaging 2001;14:23–30.
3. Kaji S, Yang PC, Kerr AB, Tang WH, Meyer CH, Macovski A, Pauly JM, Nishimura DG, Hu BS. Rapid evaluation of left ventricular volume and mass without breath-holding using real-time interactive cardiac magnetic resonance imaging system. J Am Coll Cardiol 2001;38:527–533.
4. Hori Y, Yamada N, Higashi M, Hirai N, Nakatani S. Rapid evaluation of right and left ventricular function and mass using real-time true-FISP cine MR imaging without breath-hold: comparison with segmented true-FISP cine MR imaging with breath-hold. J Cardiovasc Magn Reson 2003;5:439–450.
5. Pruessmann KP, Weiger M, Scheidegger B, Boesiger P. SENSE: sensitivity encoding for fast MRI. Magn Reson Med 1999;42:952–962.
6. Griswold MA, Jakob PM, Heidemann RM, Nittka M, Jellus V, Wang J, Kiefer B, Haase A. Generalized autocalibrating partially parallel acquisitions (GRAPPA). Magn Reson Med 2002;47:1202–1210.
7. Kellman P, Epstein FH, McVeigh ER. Adaptive sensitivity encoding incorporating temporal filtering (TSENSE). Magn Reson Med 2001;45:846–852.
8. Breuer FA, Kellman P, Griswold MA, Jakob PM. Dynamic autocalibrated parallel imaging using temporal GRAPPA (TGRAPPA). Magn Reson Med 2005;53:981–985.
9. Kellman P, Larson AC, Hsu L, Chung Y, Simonetti OP, McVeigh ER, Arai AE. Motion corrected free-breathing delayed enhancement imaging of myocardial infarction. Magn Reson Med 2005;53:194–200.
10. Ledesma-Carbayo MJ, Kellman P, Arai AE, McVeigh ER. Motion corrected free-breathing delayed enhancement imaging of myocardial infarction using non-rigid registration. J Magn Reson Imaging 2007;26:184–190.
11. Ehman RL, Felmlee JP. Adaptive technique for high definition MR imaging of moving structures. Radiology 1989;173:255–263.

12. Wang Y, Rossman PJ, Grimm RC, Riederer SI, Ehman RL. Navigator-echo-based real-time respiratory gating and triggering for reduction of respiration effects in three dimensional coronary MR angiography. Radiology 1996;198:55–60.
13. Danias PG, McConnell MV, Khasgiwala VC, Chuang ML, Edelman RR, Manning WJ. Prospective navigator correction of image position for coronary MR angiography. Radiology 1997;203:733–736.
14. Keegan J, Gatehouse P, Yang GZ, Firmin D. Coronary artery motion with the respiratory cycle during breath-holding and free-breathing: implications for slice-followed coronary artery imaging. Magn Reson Med 2002;47:476–481
15. Larson AC, Kellman P, Arai A, Hirsch GA, McVeigh E, Li D, Simonetti OP. Preliminary investigation of respiratory self-gating for free-breathing segmented cine MRI. Magn Reson Med 2005;53:159–168.
16. Stehning C, Bornert P, Nehrke K, Eggers H, Stuber M. Free-breathing whole-heart coronary MRA with 3D radial SSFP and self-navigated image reconstruction. Magn Reson Med 2005;54:476–480.
17. Lai P, Larson AC, Park J, Carr JC, Li D. Respiratory self-gated 4D coronary MRA. In: Proceedings of the 14th Annual Meeting of ISMRM, Seattle, WA, USA, 2006 (Abstract 364).
18. Uribe S, Muthurangu V, Boubertakh R, Schaeffter T, Razavi R, Hill DL, Hansen MS. Whole-heart cine MRI using real-time respiratory self-gating. Magn Reson Med 2007;57:606–613.
19. Kellman P, McVeigh ER. Image reconstruction in SNR units: a general method for SNR measurement. Magn Reson Med 2005;54:1439–1447.
20. Chefd'hotel C, Hermosillo G, Faugeras O. A variational approach to multimodal image matching. Proceedings of the IEEE Workshop on Variational and Level Set Methods in Computer Vision (VLSM'2001), ICCV Workshop, July 2001, Vancouver, BC, Canada.
21. Chefd'hotel C, Hermosillo G, Faugeras O. Flows of diffeomorphisms for multimodal image registration. Proceedings of the IEEE International Symposium on Biomedical Imaging (ISBI'2002), July 2002, Washington DC, USA.
22. Feinstein JA, Epstein FH, Arai AE, Foo TK, Hartley MR, Balaban RS, Wolff SD. Using cardiac phase to order reconstruction (CAPTOR): a method to improve diastolic images. J Magn Reson Imaging 1997;7:794–798.
23. Larson AC, White RD, Laub G, McVeigh ER, Li D, Simonetti OP. Self-gated cardiac cine MRI. Magn Reson Med 2004;51:93–102.